Chiral and Achiral Fundamental Conformational Building Units of β-Peptides: A Matrix Isolation Conformational Study on Ac-β-HGly-NHMe and Ac-β-HAla-NHMe

Tamás Beke,[†] Csaba Somlai,[‡] Gábor Magyarfalvi,[§] András Perczel,[†,∥] and György Tarczay*[,§]

Protein Modelling Group MTA-ELTE, Institute of Chemistry, Eötvös University, P.O. Box 32, H-1518, Budapest 112, Hungary, Department of Medical Chemistry, University of Szeged, Dóm tér 8, Szeged, H-6720, Hungary, Laboratory of Molecular Spectroscopy, Institute of Chemistry, Eötvös University, P.O. Box 32, H-1518, Budapest 112, Hungary, and Laboratory of Structural Chemistry and Biology, Institute of Chemistry, Eötvös University, P.O. Box 32, H-1518, Budapest 112, Hungary

Received: March 14, 2009; Revised Manuscript Received: April 21, 2009

The infrared spectra of two model β-peptides, *N*-acetyl-3-aminopropionic acid-*N*′-methylamide (Ac-β-HGly-NHMe) and *N*-acetyl-3-aminobutanoic acid-*N*′-methylamide (Ac-β-HAla-NHMe), have been recorded in low-temperature Ar and Kr matrixes. The spectra were assigned by the help of electronic structure calculations. The analysis of spectra, in line with the theoretical predictions, revealed that both biocompatible peptide building blocks have a single dominant backbone conformer. Besides this prevalent conformer, which has a six-membered H-bonded pseudoring, conformers with eight-membered H-bonded rings are also observed but in a significantly smaller amount. The calculated conformer distribution is consistent with the experimental findings. The present work along with other recent results supports the concept that the backbone conformation of longer biopolymers, such as α- and β-peptides, can be deciphered using the conformers of their structural building blocks. In this respect, our conformational study on the simplest models for β-peptides both by IR spectroscopic experiments and quantum chemical studies has significance for the better design and understanding of the backbone conformations of larger β-peptides with biomedical potential. The present conformational analysis suggests that although β-peptides, having an "extra" backbone torsion and hence more conformational freedom, should be more flexible than α-peptides, fewer backbone conformers are viable based on their relative energies. Thus, from a larger conformational arsenal, only a lower number of backbone conformers can emerge, which possibly had a fundamental effect on their applicability during prebiotic evolution.

1. Introduction

During the last two decades, there has been a rapidly increasing interest in β-peptides,[1−3] which recently became a leading target for future peptidomimetics.[4,5] From a practical, medicinal point of view, polymers composed of β-amino acid residues hold promise as potential therapeutic agents, since they provide a diversity of shape and functionality,[6,7] and they are less likely to undergo harmful metabolism. It has also been revealed that these compounds are considerably resistant to widespread proteolytic enzymes[8−10] and also have much more diverse side-chain chemistry[11] than the "natural" α-peptides.

Numerous β-amino acids and oligo-β-peptides were synthesized and investigated by various methods.[12,13] Recently, both experimental[14−22] and theoretical[23,24] studies revealed that β-peptides can adopt secondary structures, similar in fold to the natural α-peptides. Examples of such secondary structure elements include helices,[12,15,25,26] parallel and antiparallel pleated sheets,[17,19] and hairpins.[16,18,22] Surprisingly, even rather short β-peptides composed of only a few (e.g., six) residues can already fold into a definite secondary structure.[27] Further studies showed the biological potential of β-peptides, namely, their antifungal and antimicrobial activity,[28,29] cell penetrating ability,[30] or interaction with DNA duplex[31] and RNA segments.[32]

Note that several of these unique characteristics, e.g., enzymatic resistance, could be derived from the fact that β-amino acids are not in the set of fundamental building blocks for bioorganic macromolecules. However, several earlier studies showed that at least the simplest β-amino acids were present on prebiotic Earth, either from terrestrial or extraterrestrial origin.[33−36] In accordance, several reviews were published on an extensive list of natural products containing β-amino acids or other non-natural amino acids.[1,37,38] All of these observations suggest that the lack of β-amino acids in bioorganic macromolecules is the consequence of yet unrevealed factors. One such reason could be the structural differences between α- and β-amino acids, as it has been shown that, similar to the natural α-peptides composed of solely α-amino acids,[39−41] the global conformational characteristics of β-peptides can be derived from the structural properties of their building units. Thus, the survey of the basic low-energy conformers of β-amino acid diamides seems mandatory.[23,24,42−44] As shown previously, even α-amino acid diamides of simple side-chains, such as glycine (−H), alanine ($-CH_3$), etc., can adopt most basic backbone conformers, characteristic for residues of complex side chains. Interestingly, both for small peptides or large proteins, the same set of basic backbone geometries can be assigned to local minima on the potential energy surface of the above simple peptide models.[41,45] Consequently, describing the conformational building blocks of even the simplest peptide models (e.g., amino acid diamides) can serve as a good starting point to decipher higher-level structural properties of their polymers. Among

[†] Protein Modelling Group MTA-ELTE, Eötvös University.
[‡] University of Szeged.
[§] Laboratory of Molecular Spectroscopy, Eötvös University.
[∥] Laboratory of Structural Chemistry and Biology, Eötvös University.

10.1021/jp9022844 CCC: $40.75
Published on Web 05/11/2009

others,[42−44,46] some of us recently focused on the theoretical assignment of the fundamental conformers of β-amino acid diamides. It was proposed that the different backbone torsional angles of β-amino acid residues show a correlation in stable conformers, and thus they do not provide as much flexibility as is expected at first sight.[44] The systematic theoretical analysis on the β-peptide secondary structural elements[24] showed that, while β-peptides have more conformational building units than α-peptides, these are more diverse in terms of relative energy. This suggests again that in most cases there is a dominant secondary structural element for β-peptides and the conformer populations could be better balanced for α- than for β-peptides.[39] Thus, although numerous β-peptide secondary structural elements were designed and synthesized recently, their conformational availability is limited and their applicability to build macromolecules from simple amino acids might have been restricted during the prebiotic era.

Trust in these computational results depends on the theoretical level of the electronic structure method applied, and on its experimental validation. In the case of small- or medium-sized model peptides with a handful of possible conformers, such a validation is a very complex and difficult task to achieve. Nowadays, various experimental techniques, e.g., high-resolution jet-cooled laser and matrix-isolation spectroscopy, became available to provide the accurate description of the conformational ensemble of smaller flexible biomolecules.[47−49] Very recently, the conformational space of aromatic β-amino acid diamides[50] and two-residue long β-peptide triamides[51] was studied by jet-cooled double resonance UV−UV hole-burning and resonant ion dip infrared spectroscopic techniques. A great advantage of these experimental techniques is that the spectra of the unique conformers can be obtained separately, making the conformational assignment unambiguous. Furthermore, these measurements are conducted in the gas phase; thus, conformers do not have interactions with the surrounding matrix, which allows the direct comparison to quantum chemical computations also performed on isolated molecules. However, due to the nonthermodynamic equilibrium conditions in the jet-cooling process, the conformational space cannot fully be explored and several conformers of the investigated flexible molecule could be missing.[52,53] An additional drawback of these laser spectroscopic techniques is that the investigated molecules have to contain a chromophore. This requirement has far reaching consequences, as the simplest and most important achiral and chiral β-amino acid residues, which normally serve as a basis for understanding, cannot directly be investigated using the above technique. Furthermore, changing the simplest side chains to larger and aromatic ones can significantly modify the overall conformational space and hinder otherwise crucial backbone conformational building units.

In contrast to the double resonance laser spectroscopic techniques, the single conformer selection cannot easily be performed by using matrix isolation techniques, apart from special cases, e.g., investigation of photosensitive molecules.[48,54] The other disadvantage of the matrix isolation technique compared to gas-phase investigations is that the matrix can weakly interact with the molecules investigated, possibly causing a slight shift or the splitting of spectral bands. The magnitude of these effects can be estimated by recording spectra in different matrixes. At the same time, the matrix-isolation infrared (MI-IR) technique has important advantages compared to gas-phase laser techniques. As mentioned above, MI-IR investigations do not require the presence of a chromophore. Furthermore, the thermodynamic equilibrium distribution of the conformers, corresponding to the sample inlet temperature, is better conserved under the conditions of matrix isolation rather than using the jet-cooling technique. In fact, MI-IR is so powerful that only those conformers can "escape" from the matrix that can convert to lower energy forms through very low-energy (∼5 kJ mol^{-1} or lower) barriers.[48,54,55]

SCHEME 1: Constitution of the Two Investigated Basic Structural Building Units of β-Peptides with Their Three Torsional Angles Suitable to Describe the Overall Backbone Fold of These Peptides[a]

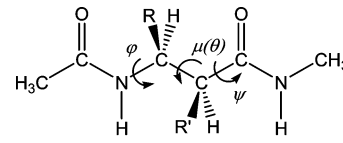

R=H, R'=H Ac-β^3-HGly-NHMe

R=CH$_3$, R'=H Ac-β^3-(*S*)-HAla-NHMe

[a] For the applied nomenclature, see Methods and refs 43 and 44.

It was shown recently that both in the case of α-amino acid diamides[55−57] and the β-amino acid residues of β-HGly (or β-Ala)[58] MI-IR spectroscopy can be an effective tool both to verify the presence of different conformers and to validate the theoretical approach taken. In the present study, we apply this method and characterize the conformational space of the simplest β-amino acid diamides (Scheme 1), namely, that of the achiral *N*-acetyl-3-aminopropionic acid-*N*′-methylamide (Ac-β-Ala-NHMe or Ac-β-HGly-NHMe) and of the chiral *N*-acetyl-3-aminobutanoic acid-*N*′-methylamide (Ac-β-Abu-NHMe or Ac-β-HAla-NHMe). Herein, we present for the first time their MI-IR spectra obtained at low temperature in Ar and Kr matrixes. The experimental analysis and the assignment of the fundamental backbone conformers were supported by electronic structure calculations. This comprehensive analysis is expected to reveal and reinforce the basic backbone structural set of β-amino acid diamides, and validate certain theoretical results obtained in the past.

2. Methods

2.1. Synthesis of the Model Compounds. The synthesis of (*S*-)Ac-β-HAla-NHMe, from (*S*-)Boc-β-HAla-OH, followed a slightly modified standard procedure.[59] Boc-β-HAla-OH (1.3 g, 6.4 mmol) and the methylammonium salt of *N*-hydroxysuccinimide (0.94 g, 6.4 mmol) was dissolved in *N*,*N*-dimethylmethanamide (DMF, 40 mL), and the mixture was cooled to 0 °C. *N*,*N*′-Dicyclohexylcarbodiimide (DCC, 1.45 g, 7.04 mmol) was added to the solution and stirred at 0 °C for 1 h and continuously another 2 h at room temperature. The mixture was concentrated in a vacuum to dryness. After addition of EtOAc (60 mL) to the remaining substance, dicyclohexylurea precipitated and was then filtered. The filtrate was washed with H_2O (30 mL), 5% $NaHCO_3$ (30 mL), and H_2O (30 mL) and dried over Na_2SO_4. The solvent was evaporated, and the crude product was crystallized from diethylether/*n*-hexane. A 830 mg (60%) portion of Boc-β-HAla-NHMe was obtained.[60]

Boc-β-HAla-NHMe (800 mg, 3.7 mmol) was dissolved in trifluoroethanoic acid (TFA, 8 mL) and H_2O (1 mL) and stirred for 1.5 h at room temperature. The solvent was evaporated, and the remaining oil was solidified by the use of diethylether. Thus, a total of 800 mg (94%) of 1:1 TFA salt of H-β-HAla-NHMe was obtained.

TFA×H-β-HAla-NHMe (800 mg, 3.47 mmol) was dissolved in DMF (6 mL), and pyridine (0.56 mL, 6.95 mmol) and Ac_2O

(0.36 mL, 3.8 mmol) were added. The mixture was stirred for 2 h at room temperature and then evaporated in a vacuum to dryness. The remaining substance was crystallized from diethylether to obtain Ac-β-HAla-NHMe (350 mg, 35%) which was purified by the use of preparative high performance liquid chromatography (HPLC, column: Phenomenex Jupiter RP C18, 10 μm, 250 $\times$ 21.2 mm, gradient elution 5−15%, 40 min; mobile phase: 80% acetonitrile, 0.1% TFA; flow rate: 4 mL min^{-1}, 220 nm). $R_f = 4.986$ (analytical column: Phenomenex Luna 5C 18(2), 250 $\times$ 4.6 mm, mobile phase: 80% acetonitrile, 0.1% TFA; flow rate: 1.2 mL min^{-1}, 220 nm). ESI-MS: Finnigan TSQ 7000: calcd, $M = 158.3$; found, $M + 1 = 159$.

Ac-β-HGly-NHMe was obtained in an analogous way, starting from the commercially available Boc-β-HGly-NH_2 purchased from Reanal.

According to analytical HPLC analysis, the purities of Ac-β-HAla-NHMe and Ac-β-HGly-NHMe were 97.1 and 99.2%, respectively (for more details, see the Supporting Information). For both samples, the purity after evaporation (see MI-IR) was also checked by HPLC and found it to be superior than 97−98%.

2.2. MI-IR Measurements. Both peptide samples were evaporated into the vacuum chamber by using a home-built Knudsen effusion cell. The cell is made of copper and heated by a heater cartridge where the temperature was measured by a thermocouple. The sample is placed inside the cell in a glass sample holder. The evaporated sample first enters into a ~0.5 cm^3 buffer chamber, and then, it leaves the cell through a variable-size pinhole. The evaporated sample was mixed with argon (Messer, 99.9997%) or krypton (Messer, 99.998%) before deposition. The gas flow was kept at 0.07 mmol min^{-1}, while the temperature of the Knudsen cell was optimized to get the shortest possible deposition time and keep the concentration low enough to minimize the formation of dimers in the matrix. The applied evaporation temperature was ~340 $\pm$ 5 K for Ac-β-HGly-NHMe and ~343 $\pm$ 5 K for Ac-β-HAla-NHMe.

The sample−rare gas mixture was deposited onto an 8−10 K CsI window mounted on a Janis CCS-350R cold head cooled by a CTI Cryogenics 22 closed-cycle refrigerator unit. The deposition time was ca. 4−8 h ($A \approx 0.4-0.8$ for the most intense band).

MI-IR spectra were recorded by a Bruker IFS 55 FT-IR spectrometer equipped with a KBr beamsplitter. A total of 1000−3000 scans were accumulated by using both DTGS and MCT detectors at 1 cm^{-1} resolution. The baseline was corrected by an adjusted polynomial function, when necessary because of interference. In the case of unresolved bands, the centers of individual transitions were determined by nonlinear curve fitting and/or Fourier deconvolution.

2.3. Computational Details. Quantum chemical calculations were performed by the PQS (Parallel Quantum Solutions) 3.2[61] and Gaussian 03 program packages.[62] Since both investigated compounds have three backbone torsional angles (Scheme 1), geometry optimization was started from grid points of the 3D Ramachandran cube[44] located at 60, 180, and −60° values of φ, μ, and ψ. Thus, this choice yielded $3^3 = 27$ starting structures. The geometry of these 27 structures was first optimized by using the Becke's three-parameter hybrid functional with the Lee−Yang−Parr correlation functional (B3LYP)[63,64] and Pople's 6-31G* basis set.[65] The obtained structures were then optimized at the B3LYP/6-311++G** level of theory. The optimizations were followed by second derivative calculations to determine whether the obtained stationary points correspond to minima. The conformers are labeled throughout this paper according to the nomenclature introduced by Möhle et al.;[43] i.e., the achiral or unsubstituted compound, Ac-β-HGly-NHMe, is labeled by **U*X***, whereas the chiral 3-amino butyric acid derivative, Ac-β-HAla-NHMe, by **B*X***, where ***X***, an integer, follows the original stability order of the conformers found by Möhle et al. for the same peptide derivative.[43,44]

In order to estimate conformational distributions, Boltzmann factors were calculated from B3LYP/6-311++G** Gibbs free energies computed for the sample inlet temperature, 340 and 343 K for the Ac-β-HGly-NHMe and Ac-β-HAla-NHMe, respectively.

Initial geometries for the transition state structure between the conformers of each possible pair have been constructed by replacing the appropriate hydrogen atoms by methyl groups on the formerly obtained transition structures of For-β-HGly-NH_2 and For-β-HAla-NH_2.[44] These transition structures of For-β-HGly-NH_2 and For-β-HAla-NH_2 were obtained by the synchronous transit-guided quasi-Newton (STQN) method[66,67] at the RHF/3-21G level of theory. The barrier heights between conformers of Ac-β-HGly-NHMe and Ac-β-HAla-NHMe were obtained by optimizing the starting geometries at the B3LYP/6-31G* level of theory by means of the traditional Berny algorithm for transition state optimizations.[66] Since there are different conformers at the RHF/3-21G and B3LYP/6-31G* levels of theory, additional transition states were searched for, by using the STQN method both for Ac-β-HGly-NHMe and Ac-β-HAla-NHMe at the B3LYP/6-31G* level of theory. All located transition structures were confirmed by one negative eigenvalue found in additional second derivative calculations at the same level of theory. Finally, in order to get better estimates for barrier heights, single point energy calculations were performed at the B3LYP/6-311++G** level of theory for the B3LYP/6-31G* transition structure geometries.

To simulate infrared spectra, harmonic vibrational frequencies and intensities were calculated at the B3LYP/6-31G* level of theory by using the scaled quantum mechanical (SQM) force field scheme[68,69] with scaling factors determined by Baker et al.[69] The 6-31G* basis set was chosen because SQM scaling factors are not yet available for larger basis sets. For spectrum simulations, Lorentzian line shapes with 3 cm^{-1} half width at half height were applied. (Computed geometries in Cartesian coordinates, vibrational frequencies and infrared transition intensities are given in the Supporting Information.)

3. Results and Discussion

3.1. Computational Results. ***Conformers of Ac-β-HGly-NHMe.*** Geometry optimizations of Ac-β-HGly-NHMe at the B3LYP/6-31G* level of theory resulted in a total of five different backbone conformational enantiomer pairs; 2 $\times$ 5 individual conformers, labeled as **U1**, **U2**, **U3**, **U4**, and **U8** with their mirror image pairs. Since the conformational enantiomers have the same energy and spectral properties, only one out of each pair is discussed. The **U8** structure is not a minimum on the B3LYP/6-311++G** potential energy surface (PES); thus, only four conformers, **U1**, **U2**, **U3**, and **U4**, exist (Table 1 and Figure 1) at the latter level of theory. The obtained structural parameters show only minor deviations from the formerly computed ones of Ac-β-HGly-NHMe[43] and For-β-HGly-NH_2[44] conformers. Unlike for the natural α-amino acid residues, here, the protecting groups affect the overall number as well as the structural properties of the conformers.

At the B3LYP/6-311++G** level of theory, **U1** is the lowest energy and the dominating conformer (Table 1). This structure is stabilized by a H-bond between the N-terminal H-atom and

TABLE 1: Selected Structural Parameters[a] and Thermochemical Data of Ac-β-HGly-NHMe Conformers Computed at the B3LYP/6-311++G Level of Theory**

conformer	φ	μ	ψ	$\Delta G^\circ_{0\,K}$[b]	$\Delta G^\circ_{340\,K}$[c]	$p_i/\Sigma p_i$[d]
U1	107	63	168	0.0	0.0	0.91
U2	−74	129	−62	6.9	11.9	0.01
U3	−107	71	10	3.5	12.4	0.01
U4	78	175	126	8.1	7.2	0.07

[a] Torsional angles (φ, μ, ψ) are in degrees, and Gibbs free (G°_T) energies are in kJ mol^{-1}. [b] Relative to **U1** at 0 K ($G^\circ_{0\,K}$ = −496.0109320 E_h). [c] Relative to **U1** at 340 K ($G^\circ_{340\,K}$ = −495.874303 E_h). [d] Boltzmann factors ($p_i/\Sigma p_i$) are calculated from $\Delta G^\circ_{340\,K}$.

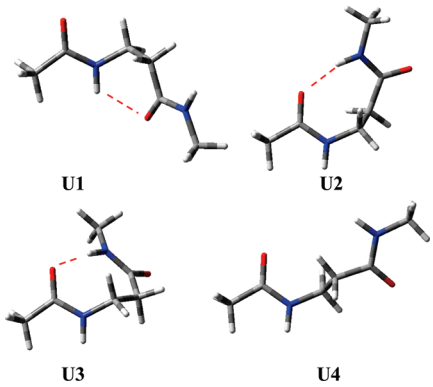

Figure 1. The four conformers of Ac-β-HGly-NHMe as optimized at the B3LYP/6-311++G** level of theory.

TABLE 2: Calculated Torsional Angles of Transition Structures (TSs) between Conformers of Ac-β-HGly-NHMe and the Corresponding Barrier Heights ($\Delta E^\#$)[a]

				$\Delta E^\#$	
TS	φ	μ	ψ	**U*i*** → **U*j***	**U*i*** ← **U*j***
U1 ↔ **U4**	76	120	162	16.9	8.8
U2 ↔ **U3**	−86	113	−38	1.4	4.8

[a] TSs are calculated at the B3LYP/6-311++G**//B3LYP/6-31G* level of theory, while conformers at the B3LYP/6-311++G** level. Torsional angles are in degrees, and barrier heights, in kJ mol^{-1}.

the C-terminal O-atom, forming a six-membered ring structure. Both the **U2** and **U3** conformers are also stabilized by an H-bond between the C-terminal H-atom and the N-terminal O-atom, forming an eight-membered pseudoring structure. The Gibbs free energies ($\Delta G^\circ_{340\,K}$) of the **U2** and **U3** conformers relative to the **U1** conformer are 11.9 and 12.4 kJ mol^{-1}, respectively. Although conformer **U4** does not form an intramolecular H-bond, partly due to its larger entropy factor, its relative $\Delta G^\circ_{340\,K}$ is not too high: 7.2 kJ mol^{-1}.

Before concluding on the expected conformer ratios in the matrix, the possible interconversion paths between conformers with their barrier heights have to be determined. Among the four conformers, **U2** and **U3** resemble each other the most, differing only in the steric alignment of their backbone ethylene groups, $-CH_2-CH_2-$. They interconvert easily through a low-energy, 1.4 kJ mol^{-1}, barrier (Table 2). As the barrier height between these two forms is low, and their Gibbs free energies are close to each other, it is possible that both of these forms are present in the matrix. Furthermore, a transition structure was located between **U1** and **U4** conformers. As it lays 8.8 and 16.9 kJ mol^{-1} above these two minima, it is likely high enough to prevent interconversion between these two conformers during depositions in the matrix. Finally, there is no direct interconversion path found between the {**U1**/**U4**} and {**U2**/**U3**} conformers. Furthermore, this conformational interconversion would require rotations around all three torsional angles, plus these conversions have a large spatial requirement; the above transitions are not expected to take place during matrix deposition.

To sum it up, most likely three conformers are expected to be present in the matrix, namely, **U1**, **U4**, and {**U2**/**U3**}. Their ratio as obtained at the B3LYP/6-311++G** level of theory is 91%, 7%, and (1+1=) 2%, respectively (Table 1). Considering the uncertainty of the calculations and the signal-to-noise level of the measurements, the dominant conformer, **U1**, should unambiguously be detected and assigned in the spectra. Furthermore, one or two additional conformers could possibly be identified, as discussed below.

TABLE 3: Selected Structural Parameters[a] and Thermochemical Data of Ac-β-HAla-NHMe Conformers Computed at the B3LYP/6-311++G Level of Theory**

conformer	φ	μ	ψ	$\Delta G^\circ_{0\,K}$[b]	$\Delta G^\circ_{340\,K}$[c]	$p_i/\Sigma p_i$[d]
B1	−138	−63	−139	0.0	0.0	0.70
B2	−70	135	−73	3.9	6.7	0.06
B2′	59	−121	81	18.1	24.5	0.00
B3′	52	52	−113	8.0	8.7	0.03
B4	61	59	−140	8.2	6.9	0.06
B5	−164	53	110	5.5	5.5	0.10
B6	−109	66	15	3.3	9.8	0.02
B8	61	163	140	13.2	12.1	0.01
B9	−99	49	85	11.5	11.2	0.01
B9′	80	−47	−92	31.8	37.1	0.00
B10	−156	65	−131	17.6	13.2	0.01
B12	−161	−67	24	28.2	30.2	0.00

[a] Torsional angles (φ, μ, ψ) are in degrees, and Gibbs free (G°_T) energies, in kJ mol^{-1}. [b] Relative to **B1** at 0 K ($G^\circ_{0\,K}$ = −535.337088 E_h). [c] Relative to **B1** at 343 K ($G^\circ_{340\,K}$ = −535.174224 E_h). [d] Boltzmann factors ($p_i/\Sigma p_i$) are calculated from $\Delta G^\circ_{340\,K}$.

Conformers of Ac-β-HAla-NHMe. In the case of Ac-β-HAla-NHMe geometry optimizations at the B3LYP/6-31G* level of theory, a total of 14 individual conformers resulted. Two among these, labeled as **B3** and **B13**, do not exist at the B3LYP/6-311++G** level of theory. Table 3 summarizes the φ, μ, and Ψ torsional angles and the Gibbs free energies of the remaining 12 conformers. Compared to previous theoretical investigations,[43,44] the obtained structural parameters show only minor deviations.

Among the 12 conformers, the two lowest energy ones, **B1** and **B5**, are stabilized by a H-bonded six-membered pseudoring structure (Figure 2). Furthermore, an additional four conformers, **B2**, **B2′**, **B3′**, and **B6**, form a H-bonded eight-membered pseudoring structure. Out of the latter four structures, **B2**, **B3′**, and **B6** lie only slightly above the global minimum of the PES; their Gibbs free energies relative to **B1** at 343 K are 6.7, 8.7, and 9.8 kJ mol^{-1}, respectively (Table 3). Due to steric repulsion, **B2′** has a relatively large Gibbs free energy, 24.5 kJ mol^{-1}. Although the six remaining conformers, **B4**, **B8**, **B9**, **B9′**, **B10**, and **B12**, form no intramolecular H-bonds, some of them, either due to dipole−dipole interaction and/or larger entropy term, have a relatively low Gibbs free energy, 6.9 kJ mol^{-1} for **B4** and around 12 kJ mol^{-1} for **B8**, **B9**, and **B10** at 343 K, respectively.

The torsional angles of the transition structures localized between conformers as well as the corresponding barrier heights are summarized in Table 4. According to these results, there is a low-energy barrier, 2−3 kJ mol^{-1}, to the **B5** conformer both from the **B9** and **B10** conformers. Therefore, these two higher energy forms might effectively be converted to **B5** during the deposition. An even lower energy barrier exists between the

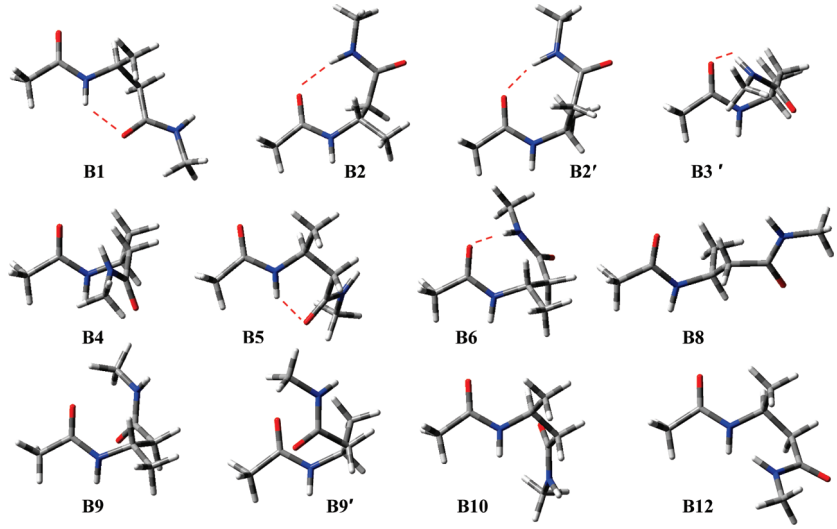

Figure 2. The 12 conformers of Ac-β-HAla-NHMe as optimized at the B3LYP/6-311++G** level of theory.

TABLE 4: Calculated Selected Torsinal Angles of Transition Structures (TSs) between Conformers of Ac-β-HAla-NHMe with the Corresponding Barrier Heights ($\Delta E^{\#}$)[a]

				$\Delta E^{\#}$	
TS	φ	μ	ψ	**B***i* → **B***j*	**B***i* ← **B***j*
B1 ↔ **B2**	−81	−125	−109	29.0	25.1
B1 ↔ **B5**	−144	−3	130	18.9	13.3
B2 ↔ **B3′**	−20	100	−105	16.9	12.9
B2 ↔ **B6**	−91	106	−32	4.2	4.8
B2′ ↔ **B4**	98	−17	106	42.8	52.7
B3′ ↔ **B4**	59	57	−133	1.0	0.8
B4 ↔ **B8**	60	115	173	14.0	9.0
B5 ↔ **B9**	−110	47	95	7.8	1.8
B5 ↔ **B10**	−169	64	−157	14.9	2.8
B3′ ↔ **B9′**	67	−12	−113	28.7	4.9

[a] TSs are calculated at the B3LYP/6-311++G**//B3LYP/6-31G* level of theory, while conformers at the B3LYP/6-311++G** level. Torsional angles are in degrees, and barrier heights, in kJ mol^{-1}.

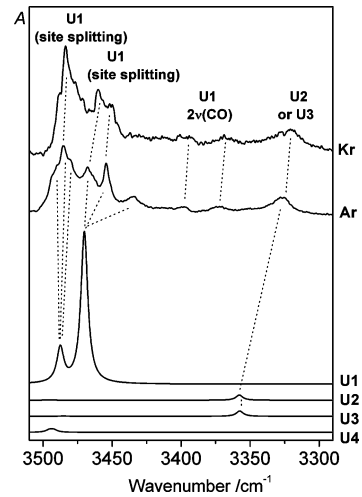

Figure 3. Amide A region of matrix IR spectra of Ac-β-HGly-NHMe and the Boltzmann-weighted computed spectra of the individual conformers.

B4 and **B3′** conformers, and a slightly higher one, 4−5 kJ mol^{-1}, between the **B2** and **B6** conformers. Since **B4** and **B3′** as well as **B2** and **B6** are close in energy, the order of their relative Gibbs free energy is temperature dependent. Furthermore, as their backbone structures are similar, either all of these structures or one of the pairs could coexist in the matrix. The other barrier heights listed in Table 4 either are too high to allow a conversion during the deposition or connect high-energy conformers only, abundances of which are computed to be negligible at deposition temperature.

According to the above results, the **B1** and **B5** conformers should be the most abundant structures in the matrix. Since their predicted abundances, ∼70% and (10+1+1=) 12%, respectively, are well above the detection limit, they are expected to be unambiguously identified in the matrix. The {**B4**/**B3′**} as well as the {**B2**/**B6**} forms could also be present in an observable amount. Finally, the computed abundance of all of the other conformers is comparable to the amount of impurities or well below the detection limit. Hence, these conformers are not attempted to be identified during the spectrum analysis.

3.2. Spectral Analysis. *Ac-β-HGly-NHMe.* The most informative amide A, I, and II regions of the experimental spectra together with the computed spectra of each dominant conformer are shown in Figures 3 and 4. (All additional spectral regions can be found in the Supporting Information.) The most intensive bands of the experimental spectrum correlate very well with the calculated band positions and intensities of the **U1** conformer of Ac-β-HGly-NHMe. After accounting for all of the fundamental and possible overtone transitions of the **U1** conformer, some medium and weak intensity bands (e.g., at 3326, 1680, and 1555 cm^{-1} in Ar) remain unassigned. Since the majority of these spectral features look the same or rather similar in Ar and Kr matrixes, they cannot be caused by site splitting effects. Furthermore, these bands are reproduced independently of the deposition conditions (e.g., water content, slight variation of the evaporation temperature); thus, they cannot be identified as peptide dimers or peptide−water complexes. Finally, they are too intensive to assign them as contaminants, present less than 1% in the matrix (see Methods). The eluent TFA was also considered, and measured independently in Ar matrix. Clearly, only a few of its most intensive bands are detectable in the spectrum of Ac-β-HGly-NHMe. In conclusion, these bands must be present due to the minor conformers.

In the N−H stretching region (Figure 3), the bands above 3400 cm^{-1} can be assigned to the two amide A modes of the dominant **U1** conformer (Table 5). Due to site splitting effects, which often appear in this region, the experimental spectrum is more complex. Comparing the calculated intensities of the two amide A modes of **U1**, it is likely that the lower frequency mode

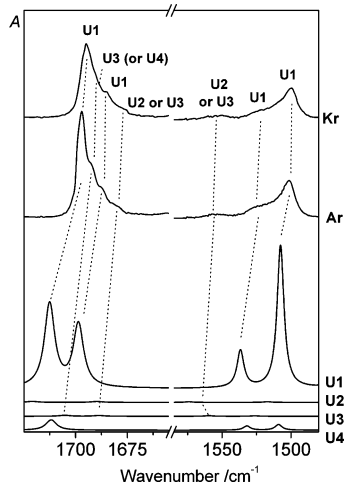

Figure 4. Amide I and II regions of matrix IR spectra of Ac-β-HGly-NHMe and the Boltzmann-weighted computed spectra of the individual conformers.

TABLE 5: Observed Amide A, I, and II Band Positions (in cm^{-1}) of Ac-β-HGly-NHMe and Their Assignments[a]

Ar	Kr	assignment
3485,[b] 3491,[b,c] 3480[b,c]	3484,[b] 3488,[b,c] 3476,[b,c] 3471[b,c]	**U1** ν_1
3467,[b] 3454,[b] 3434[b]	3466,[b,c] 3460,[b] 3451,[b] 3447[b,c]	**U1** ν_2
3398	3395	**U1** $2\nu_{13}$
3373	3368	**U1** $2\nu_{14}$
3326	3320	**U3** ν_2 and/or **U2** ν_2
1697	1695	**U1** ν_{13} (and **U4** ν_{13})
1692	1690	**U3** ν_{13}
1687	1685	**U1** ν_{14}
1680	1677	**U3** ν_{14} and/or **U2** ν_{14}
1555	1552	**U3** ν_{15} and/or **U2** ν_{15}
1526	1521	**U1** ν_{15}
1512	1509	**U3** ν_{16}
1501	1500	**U1** ν_{16}

[a] Assigment of the other spectral regions can be found in the Supporting Information. [b] Site splitting. [c] Low-intensity band or shoulder.

is split into three bands in Ar. This assignment is supported by the Kr matrix measurements, where the structure of this feature looks different; i.e., it is split into two bands only. The contribution of the higher frequency amide A modes introduces further complexity in the structure of this group of bands. There are two weak bands at 3398/3395 and 3373/3368 cm^{-1} in Ar/Kr. These can be identified as the overtones of amide A modes of the most abundant **U1** conformer. The lowest frequency transition in the amide A region is at 3326/3320 cm^{-1} in Ar/Kr. Among the computed vibrational transitions, only the lower frequency amide A band of **U2** and **U3** can be matched to this experimental band position.

Similarly to the amide A region, in all of the other spectral regions, including amide I and amide II regions (Figure 4), the dominant features are easy to assign to the **U1** conformer. There are many weak shoulders or well separated weak bands, whose positions and intensities are in good correspondence with the computed band positions and intensities of **U2** and **U3** structures. Although the computed **U3** spectrum correlates somewhat better with these bands, it is impossible to exclusively identify them with either the transitions of **U2** or those of **U3**. Nevertheless, the structure present in the matrix might either be **U2** and/or **U3** or a structure very similar to both **U2** and **U3** but slightly distorted by the matrix.

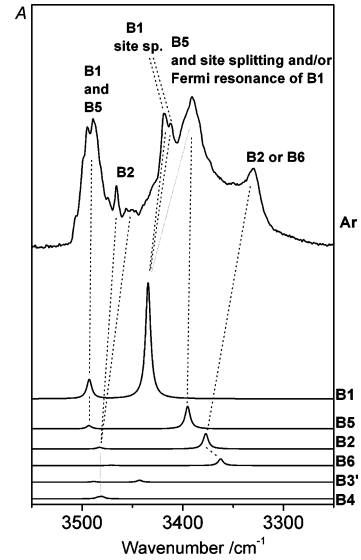

Figure 5. Amide A region of the matrix IR spectrum of Ac-β-HAla-NHMe and the Boltzman-weighted computed spectra of the individual conformers.

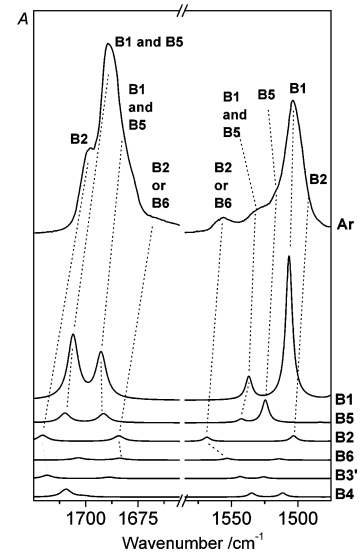

Figure 6. Amide I and II regions of the matrix IR spectrum of Ac-β-HAla-NHMe and the Boltzman-weighted computed spectra of the individual conformers.

Some bands of very weak intensity are left after the full assignment of the transitions of **U1** and {**U2/U3**}. In the amide A, I, and II regions, the computed bands of **U4** overlap almost perfectly with the intensive absorption bands of **U1**. In other regions (see the Supporting Information), the intensity of the bands, which might be assigned to **U4**, are comparable with the intensities of possible contaminations; thus, the presence of this conformer cannot be seen as proven.

In conclusion, on the basis of the similarity of the computed and observed intensities, the computed relative abundance of **U1** and {**U2/U3**} is in qualitative agreement with the observed data.

Ac-β-HAla-NHMe. Most of the intensive bands of the vibrational spectrum of Ac-β-HAla-NHMe can unambiguously be assigned to the **B1** conformer (Figures 5−7, Table 6). In these figures, only the computed and Ar matrix spectra are displayed. Kr matrix spectra as well as other regions of the spectra can be found in the Supporting Information. The remaining unassigned bands, based on similar arguments that

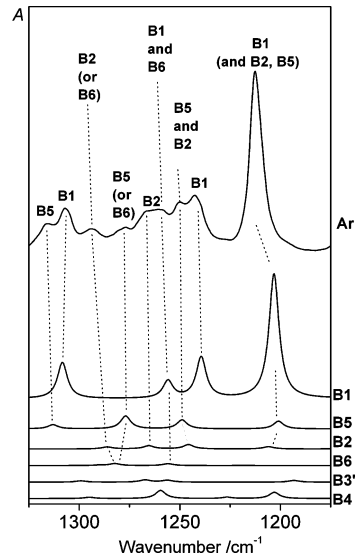

Figure 7. The 1175−1325 cm^{-1} region of the matrix IR spectrum of Ac-β-HAla-NHMe and the Boltzman-weighted computed spectra of the individual conformers.

TABLE 6: Observed Amide A, I, II, and Some Further Band Positions (in cm^{-1}) of Ac-β-HAla-NHMe and Their Assignments[a]

Ar	Kr	assignment
3506,[b,c] 3495,[b] 3488,[b] 3475[b,c]	3491,[b,c] 3485,[b] 3480[b]	**B1** ν_1 and **B5** ν_1
3466,[b] 3456,[b,c] 3450[b]	3465,[b] 3457,[b,c] 3447[b]	**B2** ν_1 (or **B4** ν_1 and ν_2)
3428,[b,c] 3419,[b] 3412[b]	3429,[b,c] 3417[b]	**B1** ν_2
3390[b]	3391,[b] 3381,[b,c] 3369[b,c]	**B1** ν_2 and/or **B5** ν_2
3329	3325	**B2** ν_2 (and/or **B6** ν_2)
1699	1696	**B2** ν_{15}
1690	1685	**B1** ν_{15} (and **B5** ν_{15})
1680	1676	**B1** ν_{16} (and **B5** ν_{16})
1668	1669	**B2** ν_{16} (and/or **B6** ν_{16})
1556	1559	**B2** ν_{17} (and/or **B6** ν_{17})
1531	1520[d]	**B1** ν_{17} and **B5** ν_{17}
1516	1520[d]	**B5** ν_{18}
1503	1501	**B1** ν_{18}
1491	1489	**B2** ν_{18}
1316	1314	**B5** ν_{31}
1307	1305	**B1** ν_{31}
1294	1292	**B2** ν_{31} (and/or **B6** ν_{32})
1278	1279	**B5** ν_{32} (and/or **B6** ν_{32})
1266	1266	**B2** ν_{32}
1260	1259	**B1** ν_{32} (and **B6** ν_{33})
1250	1248	**B2** ν_{33} and **B5** ν_{33}
1242	1241	**B1** ν_{33}
1213	1212	**B1** ν_{34} (and **B2** ν_{34} and **B6** ν_{34})

[a] Assigment of the other spectral regions can be found in the Supporting Information. [b] Low-intensity band or shoulder. [c] Site splitting. [d] Unresolved.

were given for Ac-β-HGly-NHMe, must belong to the minor conformers. Accounting for all of the possible overtones and site splittings, at least two minor conformers must be present in a considerable amount. During the assignment of these remaining bands, only the conformers predicted by the calculations to have an abundance of more than 2%, namely, the {**B2/B6**}, {**B4/B3′**}, and **B5** conformers, were considered.

Some of the bands not assigned to the **B1** conformer can confidently be identified as the vibrational transitions of either the **B2** or **B6** conformer. These are the bands observed in Ar matrix, e.g., at 3329, 1556, 740, and 729 cm^{-1}. The assignment of these bands to any of the other three conformers is unreasonable based on their calculated band positions and intensities. (See Figures 5−7, as well as the calculated band positions and intensities of each conformer in the Supporting Information.) The other computed bands of the **B2** and **B6** conformers, both in position and intensity, correspond well to some bands not assigned to the **B1** conformer. Since the structure of **B2** and **B6** and consequently the key features of their computed spectra are rather similar, it is impossible to decide which one exists in the matrix. As is concluded in section 3.1, probably a similar structure, slightly distorted from both **B2** and **B6**, is present due to the interaction with the host matrix.

The number of observed bands, especially in the fingerprint region (Figure 7), indicates that at least one more conformer should be present in a detectable amount. The bands still remaining after assigning the bands of the **B1** and {**B2/B6**} conformers correlate the best with the computed **B5** spectrum (e.g., the shoulder at 1516 cm^{-1}, as well as the bands at 1316 and 1278 cm^{-1} in Ar; see Figures 6 and 7). The identification of **B5** is somewhat less certain than that of **B1** and {**B2/B6**}.

When all of the computed bands of **B5** are correlated with the experimental observations, very weak features remain in the Ar (and Kr) matrix spectra assigned neither to **B1** and {**B2/B6**} nor to **B5**. In principle, these can be the vibrational transitions of the **B4** or **B3′** conformers, but considering their low intensity and the ∼2% possible contamination, they cannot be safely identified.

In summary, the dominant **B1** conformer can unambiguously be identified in the spectra. There are at least two additional conformers in the matrix in an observable amount. These two conformers are most likely the {**B2/B6**} and **B5** structures. Comparing the intensities, scaled by the computed Boltzmann-weighted factors, the experimental observations qualitatively agree with the calculated conformer ratios. The {**B2/B6**} conformers might be slightly more, while the {**B4/B3′**} conformers are probably somewhat less abundant in the matrix than it is calculated.

3.3. Conclusions. In this study, the major conformers of the simplest achiral and chiral β-amino acid diamides, Ac-β-HGly-NHMe and Ac-β-(*S*)-HAla-NHMe, were investigated using matrix isolation infrared spectroscopy combined with quantum chemical calculations. The results undoubtedly indicate that multiple conformers are present in both model systems.

In the case of the achiral β-peptide building unit, the **U1** conformer, strongly stabilized by a six-membered H-bonded pseudoring, is dominant. Furthermore, a pair of eight-membered H-bond conformers {**U2/U3**}, connected with a low energy interconversion pathway (Table 2), can also be assigned in the spectra, as predicted by the calculations. Similarly, in the case of the simplest chiral building block of β-peptides, Ac-β-HAla-NHMe conformer **B1** with a six-membered H-bonded ring dominates the spectra. Furthermore, additional conformers with cyclic H-bonded rings, namely, **B5** (six-membered) and {**B2/B6**} (easily converting eight-membered rings), can be assigned in the spectra. The computed Boltzmann-weighted intensities and the experimental band intensities of the conformers agree qualitatively. Our present results support the structural information recently obtained on chiral, aromatic β-amino acid diamides by using jet-cooled double resonance UV−UV hole-burning and resonant ion dip infrared spectroscopic techniques,[50] where also a six- and an eight-membered H-bonded structure was found to be prevalent in the gas phase.

One further outcome of this work is that the theoretical backbone geometries obtained are very similar to those of the chiral β-amino acids with different side chains.[50] Namely, the

average difference between the backbone torsional angles of the corresponding β-HPhe and β-HAla conformers is only 3.7°. These results suggest that, as for α-peptides, the conformational characterization of β-peptides can be achieved by determining the conformational properties of the simplest chiral and achiral building units. For β-amino acids, however, the conformers are less evenly distributed than for α-amino acids.[55] While natural α-amino acid peptide models have fewer backbone conformers, there are at least two but often more backbone structures (e.g., β_L, γ_L, and γ_D) among them in the conformational ensemble with a Boltzmann fraction higher than 0.15−0.20.[55] In contrast to the above, for the β-peptide models investigated here, the molecular systems present an ill-balanced conformational equilibrium, so that besides the dominant conformer (∼90%) the second and the additional most populated conformer(s) have only a minor contribution (around or less than 5%). This observation, in line with our previous theoretical results,[44] suggests that the conformational ensemble of the backbone structural building units is more strongly energy filtered for β- than it is for α-peptides. Thus, the exclusion of a large section of the conformational space reduces the inherent flexibility of these backbones. It seems that this type of polymer becomes rigid "too early" (i.e., in an early phase of oligomerization). Thus, perhaps for this reason, they have been eliminated from the set of natural building blocks during molecular evolution, being ineffective in forming cooperative nanostructures. This could be the explanation why β-peptides and "β-proteins" were not adaptive enough during the prebiotic era. Nevertheless, their negligible evolutionary role provided great enzymatic resistance, which combined with such structural "rigidity" promises that artificially designed β-peptides could play a major role among biomimetics because of their very nature.

Acknowledgment. This work was funded by the Hungarian Scientific Research Fund (OTKA F042722, K72973, NI-68466) and by International Centre for Genetic Engineering and Biotechnology (ICGEB Hun08-03). The ELTE Computer Facility and the HPC group at University of Szeged were used to complete some of the calculations. G.T. was supported by the János Bolyai Research Scholarship of the Hungarian Academy of Sciences.

Supporting Information Available: HPLC analyses, the optimized geometries and transition structures, the scaled vibrational frequencies, the MI-IR spectra in the full spectral range, and the tentative assignments. This material is available free of charge via the Internet at http://pubs.acs.org.

References and Notes

(1) Seebach, D.; Beck, A. K.; Bierbaum, D. J. *Chem. Biodiversity* **2004**, *1*, 1111–1239.

(2) Nielsen, P. E. *Pseudo-Peptides in Drug Discovery*; Wiley-VCH: Weinheim, Germany, 2004; pp 33−113.

(3) Apella, D. H.; Christianson, L. A.; Klein, D. A.; Powell, D. R.; Hunag, X. L.; Barchi, J. J., Jr.; Gellman, S. H. *Nature* **1997**, *387*, 381–384.

(4) Seebach, D.; Gardiner, J. *Acc. Chem. Res.* **2008**, *41*, 1366–1375.

(5) Horne, W. S.; Gellman, S. H. *Acc. Chem. Res.* **2008**, *41*, 1399–1408.

(6) Kritzer, J. A.; Stephens, O. M.; Guarracino, D. A.; Reznik, S. K.; Schepartz, A. *Bioorg. Med. Chem.* **2005**, *13*, 11–16.

(7) Mengel, A.; Reiser, O.; Aube, J. *Bioorg. Med. Chem. Lett.* **2008**, *18*, 5975–5977.

(8) Frackenpohl, J.; Arvidsson, P. I.; Schreiber, J. V.; Seebach, D. *ChemBioChem* **2001**, *2*, 445–455.

(9) Hintermann, T.; Seebach, D. *Chimia* **1997**, *51*, 244–247.

(10) Seebach, D.; Albert, M.; Arvidsson, P. I.; Rueping, M.; Schreiber, J. V. *Chimia* **2001**, *55*, 345–353.

(11) Seebach, D.; Abele, S.; Gademann, K.; Guichard, G.; Hintermann, T.; Jaun, B.; Matthews, J. L.; Schreiber, J. V. *Helv. Chim. Acta* **1998**, *81*, 932–982.

(12) DeGrado, W. F.; Hamuro, Y.; Schneider, J. P. *J. Peptide Res.* **1999**, *54*, 206–217.

(13) Fülöp, F. *Chem. Rev.* **2001**, *101*, 2181–2204.

(14) Martinek, T. A.; Tóth, G. K.; Vass, E.; Hollósi, M.; Fülöp, F. *Angew. Chem., Int. Ed.* **2002**, *41*, 1718–1721.

(15) Seebach, D.; Overhand, M.; Kuhnle, F. N. M.; Martinoni, B.; Oberer, L.; Hommel, U.; Widmer, H. *Helv. Chim. Acta* **1996**, *79*, 913–941.

(16) Seebach, D.; Abele, S.; Gademann, K.; Jaun, B. *Angew. Chem., Int. Ed.* **1999**, *38*, 1595–1597.

(17) Krauthauser, S.; Christianson, L. A.; Powell, D. R.; Gellman, S. H. *J. Am. Chem. Soc.* **1997**, *119*, 11719–11720.

(18) Karle, I.; Gopi, H. N.; Balaram, P. *Proc. Natl. Acad. Sci. U.S.A.* **2002**, *99*, 5160–5164.

(19) Chung, Y. J.; Huck, B. R.; Christianson, L. A.; Stanger, H. E.; Krauthauser, S.; Powell, D. R.; Gellman, S. H. *J. Am. Chem. Soc.* **2000**, *122*, 3995–4004.

(20) Diederichsen, U.; Schmitt, H. W. *Eur. J. Org. Chem.* **1998**, *1998*, 827–835.

(21) Chung, Y. J.; Christianson, L. A.; Stanger, H. E.; Powell, D. R.; Gellman, S. H. *J. Am. Chem. Soc.* **1998**, *120*, 10555–10556.

(22) Daura, X.; Gademann, K.; Schafer, H.; Jaun, B.; Seebach, D.; van Gunsteren, W. F. *J. Am. Chem. Soc.* **2001**, *123*, 2393–2404.

(23) Günther, R.; Hofmann, H. J.; Kuczera, K. *J. Phys. Chem. B* **2001**, *105*, 5559–5567.

(24) Beke, T.; Somlai, C.; Perczel, A. *J. Comput. Chem.* **2006**, *27*, 20–38.

(25) Hetényi, A.; Szakonyi, Z.; Mándity, I. M.; Szolnoki, É.; Tóth, G. K.; Martinek, T. A.; Fülöp, F. *Chem. Commun.* **2009**, *2*, 177–179.

(26) Appella, D. H.; Christianson, L. A.; Karle, I. L.; Powell, D. R.; Gellman, S. H. *J. Am. Chem. Soc.* **1996**, *118*, 13071–13072.

(27) Seebach, D.; Matthews, J. L. *Chem. Commun.* **1997**, 2015–2022.

(28) Ziegelbauer, K. *Antimicrob. Agents Chemother.* **1998**, *42*, 1581–1586.

(29) Porter, E. A.; Weisblum, B.; Gellman, S. H. *J. Am. Chem. Soc.* **2002**, *124*, 7324–7330.

(30) Rueping, M.; Mahajan, Y.; Sauer, M.; Seebach, D. *ChemBioChem* **2002**, *3*, 257–259.

(31) Namoto, K.; Gardiner, J.; Kimmerlin, T.; Seebach, D. *Helv. Chim. Acta* **2006**, *89*, 3087–3103.

(32) Gelman, M. A.; Richter, S.; Cao, H.; Umezawa, N.; Gellman, S. H.; Rana, T. M. *Org. Lett.* **2003**, *5*, 3563–3565.

(33) Miller, S. L. *Science* **1953**, *117*, 528–529.

(34) Oró, J. *Nature* **1961**, *190*, 389–390.

(35) Barak, I.; Bar-Nun, A. *Orig. Life* **1975**, *6*, 483–506.

(36) Ehrenfreund, P.; Glavin, D. P.; Botta, O.; Cooper, G.; Bada, J. L. *Proc. Natl. Acad. Sci. U.S.A.* **2001**, *98*, 2138–2141.

(37) Drey, C. N. C. The Chemistry and Biochemistry of β-Amino Acids. In *Chemistry and Biochemistry of Amino Acids, Peptides and Proteins*; Weinstein, B., Ed.; M. Dekker: New York, 1977; Vol. 4, pp 241−299.

(38) Lelais, G.; Seebach, D. *Biopolymers* **2004**, *76*, 206–243.

(39) Perczel, A.; Jákli, I.; Csizmadia, I. G. *Chem.—Eur. J.* **2003**, *9*, 5332–5342.

(40) Perczel, A.; Gáspári, Z.; Csizmadia, I. G. *J. Comput. Chem.* **2005**, *26*, 1155–1168.

(41) Perczel, A.; Ángyán, J. G.; Kajtár, M.; Viviani, W.; Rivail, J. L.; Marcoccia, J. F.; Csizmadia, I. G. *J. Am. Chem. Soc.* **1991**, *113*, 6256–6265.

(42) Günther, R.; Hofmann, H. J. *Helv. Chim. Acta* **2002**, *85*, 2149–2168.

(43) Möhle, K.; Günther, R.; Thormann, M.; Sewald, N.; Hofmann, H. J. *Biopolymers* **1999**, *50*, 167–184.

(44) Beke, T.; Csizmadia, I. G.; Perczel, A. *J. Comput. Chem.* **2004**, *25*, 285–307.

(45) Head-Gordon, T.; Head-Gordon, M.; Frisch, M. J.; Brooks, C. L.; Pople, J. A. *J. Am. Chem. Soc.* **1991**, *113*, 5989–5997.

(46) Láng, A.; Füzéry, A. K.; Beke, T.; Hudáky, P.; Perczel, A. *THEOCHEM* **2004**, *675*, 163–175.

(47) Zwier, T. S. *J. Phys. Chem. A* **2006**, *110*, 4133–4150, and references therein.

(48) Barnes, A. J. *J. Mol. Struct.* **1984**, *113*, 161–174, and references therein.

(49) Klaeboe, P. *Vib. Spectrosc.* **1995**, *9*, 3–17, and references therein.

(50) Baquero, E. E.; James, W. H.; Choi, S. H.; Gellman, S. H.; Zwier, T. S. *J. Am. Chem. Soc.* **2008**, *130*, 4784–4794.

(51) Baquero, E. E.; James, W. H.; Choi, S. H.; Gellman, S. H.; Zwier, T. S. *J. Am. Chem. Soc.* **2008**, *130*, 4795–4807.

(52) Zehnacker, A.; Suhm, M. A. *Angew. Chem., Int. Ed.* **2008**, *47*, 6970–6992.

(53) Godfrey, P. D.; Brown, R. D.; Rodgers, F. M. *J. Mol. Struct.* **1996**, *376*, 65–81.
(54) Mátyus, E.; Magyarfalvi, G.; Tarczay, G. *J. Phys. Chem. A* **2007**, *111*, 450–459.
(55) Pohl, G.; Perczel, A.; Vass, E.; Magyarfalvi, G.; Tarczay, G. *Tetrahedron* **2008**, *64*, 2126–2133.
(56) Pohl, G.; Perczel, A.; Vass, E.; Magyarfalvi, G.; Tarczay, G. *Phys. Chem. Chem. Phys.* **2007**, *9*, 4698–4708.
(57) Tarczay, G.; Góbi, S.; Vass, E.; Magyarfalvi, G. *Vib. Spectrosc.* **2009**, *50*, 21−28.
(58) Dobrowolski, J. Cz.; Jamróz, M. H.; Kołos, R.; Rode J. E.; Sadlej, J. *ChemPhysChem* **2008**, *9*, 2042−2051.
(59) Penke, B.; Czombos, J.; Baláspiri, L.; Petres, J.; Kovács, K. *Helv. Chim. Acta* **1970**, *53*, 1057–1061.
(60) Somlai, C.; Szókán, G.; Baláspiri, L. *Synthesis* **1992**, 285–287.
(61) *PQS*, version 3.2; Parallel Quantum Solutions: Fayetteville, AR.
(62) Frisch, M. J.; Trucks, G. W.; Schlegel, H. B.; Scuseria, G. E.; Robb, M. A.; Cheeseman, J. R.; Montgomery, J. A., Jr.; Vreven, T.; Kudin, K. N.; Burant, J. C.; Millam, J. M.; Iyengar, S. S.; Tomasi, J.; Barone, V.; Mennucci, B.; Cossi, M.; Scalmani, G.; Rega, N.; Petersson, G. A.; Nakatsuji, H.; Hada, M.; Ehara, M.; Toyota, K.; Fukuda, R.; Hasegawa, J.; Ishida, M.; Nakajima, T.; Honda, Y.; Kitao, O.; Nakai, H.; Klene, M.; Li, X.; Knox, J. E.; Hratchian, H. P.; Cross, J. B.; Bakken, V.; Adamo, C.; Jaramillo, J.; Gomperts, R.; Stratmann, R. E.; Yazyev, O.; Austin, A. J.; Cammi, R.; Pomelli, C.; Ochterski, J. W.; Ayala, P. Y.; Morokuma, K.; Voth, G. A.; Salvador, P.; Dannenberg, J. J.; Zakrzewski, V. G.; Dapprich, S.; Daniels, A. D.; Strain, M. C.; Farkas, O.; Malick, D. K.; Rabuck, A. D.; Raghavachari, K.; Foresman, J. B.; Ortiz, J. V.; Cui, Q.; Baboul, A. G.; Clifford, S.; Cioslowski, J.; Stefanov, B. B.; Liu, G.; Liashenko, A.; Piskorz, P.; Komaromi, I.; Martin, R. L.; Fox, D. J.; Keith, T.; Al-Laham, M. A.; Peng, C. Y.; Nanayakkara, A.; Challacombe, M.; Gill, P. M. W.; Johnson, B.; Chen, W.; Wong, M. W.; Gonzalez, C.; Pople, J. A. *Gaussian 03*, revision C.02; Gaussian, Inc.: Wallingford, CT, 2004.
(63) Becke, A. D. *J. Chem. Phys.* **1993**, *98*, 5648–5652.
(64) Lee, C.; Yang, W.; Parr, R. G. *Phys. Rev. B* **1988**, *37*, 785–789.
(65) Hehre, W. J.; Ditchfield, R.; Pople, J. A. *J. Chem. Phys.* **1972**, *56*, 2257–2261.
(66) Peng, C. Y.; Ayala, P. Y.; Schlegel, H. B.; Frisch, M. J. *J. Comput. Chem.* **1996**, *17*, 49–56.
(67) Peng, C. Y.; Schlegel, H. B. *Isr. J. Chem.* **1993**, *33*, 449–454.
(68) Pulay, P.; Fogarasi, G.; Pongor, G.; Boggs, J. E.; Vargha, A. *J. Am. Chem. Soc.* **1983**, *105*, 7037–7047.
(69) Baker, J.; Jarzecki, A. A.; Pulay, P. *J. Phys. Chem. A* **1998**, *102*, 1412–1424.

JP9022844